Available online at www.sciencedirect.com

ScienceDirect

Mathematics and Computers in Simulation 79 (2008) 1051–1059

MATHEMATICS AND COMPUTERS IN SIMULATION

www.elsevier.com/locate/matcom

Numerical study of quantum transport in carbon nanotube transistors

M. Pourfath *, H. Kosina, S. Selberherr

Institute for Microelectronics, TU Wien, Gußhausstraße 27–29/E360, 1040 Wien, Austria

Received 16 September 2007; accepted 18 September 2007
Available online 25 September 2007

Abstract

A deeper understanding of quantum effects in nano-electronic devices helps to improve the functionality and to develop new device types. The performance of carbon nanotube (CNT) field-effect transistor is studied using the non-equilibrium Green's function (NEGF) formalism. The effects of elastic and inelastic scattering and the impact of parameters, such as electron–phonon coupling strength and phonon energy, on the device performance are analyzed.
© 2007 IMACS. Published by Elsevier B.V. All rights reserved.

PACS: 61.46.Fg; 85.35.Kt; 63.20.Kr

Keywords: Nanotube transistors; Electron–phonon interaction; Quantum transport

1. Introduction

Tremendous advances have been achieved in microelectronics technology during the past decades. With continuing efforts to improve speed and functionality of integrated circuits and to achieve higher integration densities, device dimensions are decreased and eventually reach the scale of the electron wavelength. With the aid of numerical analysis one can gain a deeper insight into device operation and investigate methods to improve the device performance.

A carbon nanotube (CNT) can be viewed as a rolled-up sheet of graphene with a diameter of a few nano-meters. The way the graphene sheet is wrapped is represented by a pair of indices (n, m) called the chiral vector. The integers n and m denote the number of basis vectors along two directions in the honeycomb crystal lattice of graphene. The CNT is called *zigzag*, if $m = 0$, *armchair*, if $n = m$, and *chiral* otherwise. CNTs with $n - m = 3$ are metals, otherwise they are semiconductors [22]. Semiconducting CNTs can be used as channels for transistors [18] which have been studied in recent years as potential alternatives to CMOS devices because of their capability of ballistic transport.

Depending on the work function difference between the metal contact and the CNT, carriers at the metal–CNT interface encounter different barrier heights (see Fig. 1). Fabrication of devices with positive (Schottky type) [1] and zero (Ohmic) [11] barrier heights for holes have been reported. In this work we consider devices with zero barrier heights for electrons.

* Corresponding author.
E-mail address: pourfath@iue.tuwien.ac.at (M. Pourfath).

0378-4754/$32.00 © 2007 IMACS. Published by Elsevier B.V. All rights reserved.
doi:10.1016/j.matcom.2007.09.004

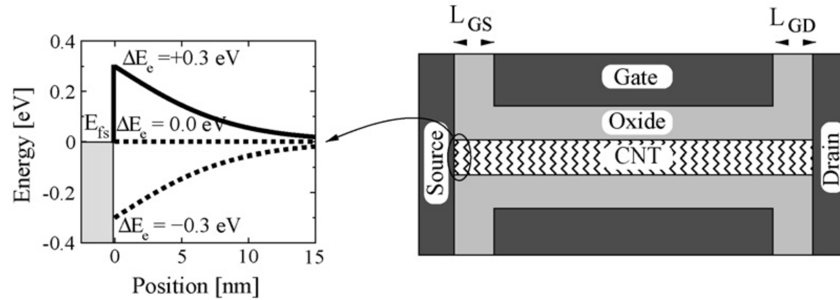

Fig. 1. Sketch of the CNTFET investigated. The insulating layer is HfO_2 with $\epsilon_r = 15$ and a thickness of 2 nm. $L_{GS} = L_{GD} = 4$ nm and $L_{CNT} = 50$ nm.

The non-equilibrium Green's function (NEGF) method has been successfully utilized to investigate the characteristics of nano-scale silicon transistors [24], carbon nanotube based transistors [23], and molecular devices [25,27]. In this work we employ the NEGF formalism to study quantum transport in CNT based transistors in more detail.

2. Governing equations

The NEGF technique initiated by Schwinger and Kadanoff and Baym allows one to study the time evolution of a many-particle quantum system. Knowing the single-particle Green's functions of a given system, one may evaluate single-particle quantities like carrier density or current. The many-particle information about the system is cast into self-energies, which are part of the equations of motion for the Green's functions. Perturbation expansion of the Green's functions is the key to approximate the self-energies. Green's functions provide a powerful technique to evaluate the properties of a many-body system both in thermodynamic equilibrium and non-equilibrium situations. A non-equilibrium condition can occur due to for example an applied electric field, a light excitation pulse, or coupling to contacts at different (electro) chemical potentials.

2.1. The non-equilibrium green's function

Four types of Green's functions are defined: the retarded and advanced Green's functions, $G^{\mathrm{r,a}}$, deal with the dynamics of carriers and lesser and greater Green's functions, $G^{\lessgtr}$, with the statistics. The transport equations are solved on the surface of the CNT. Due to quantum confinement along the tube circumference, wavefunction of carriers are bound around the CNT and can propagate along the tube axis. We considered an azimuthal symmetric structure, in which the gate fully surrounds the CNT. Under the assumption that the potential profile does not vary sharply along the CNT, sub-bands are decoupled [26]. As a result, transport equations need to be solved only along the CNT axis which is assumed to be the z direction in cylindrical coordinates. In this work we assume bias conditions for which the first sub-band contributes mostly to the total current. In the mode-space approach the transport equation for each sub-band can be written as [23,3]

$$G^{\mathrm{r,a}}(z, z'; E) = [EI - H(z, z'; E) - \Sigma^{\mathrm{r,a}}(z, z'; E)]^{-1}, \tag{1}$$

$$G^{\lessgtr}(z, z'; E) = G^{\mathrm{r}}(z, z'; E)\Sigma^{\lessgtr}(z, z'; E)G^{\mathrm{a}}(z, z'; E), \tag{2}$$

where the self-energy Σ describes the renormalization of the Green's function due to the interaction with the surrounding many-particle system, H is the single-particle Hamiltonian. The general form of the single-particle Hamiltonian is given by

$$H(z) = -\frac{\hbar^2}{2m}\nabla_z + U(z), \tag{3}$$

where H contains the kinetic energy and the potential energy U which includes the effects of the band structure and the Hartree potential which is in fact the solution of the Poisson equation.

2.2. Boundary conditions and contact self-energies

In order to solve the system of equations discussed above in a finite system, boundary conditions have to be specified. The boundary conditions of (1) have to model the contacts, which act as a source or drain for electrons. Due to the transitions between the device and the lead, this type of boundary condition can be demonstrated by adding contact self-energies to the total self-energy [24,16,3]. The self-energies due to contacts are only non-zero at the boundaries [3]

$$\Sigma_{\mathrm{c}}^{\mathrm{r}}(E) = \tau^2 g_{\mathrm{c}}, \tag{4}$$

$$\Sigma_{\mathrm{c}}^{<}(E) = -2i\Im m[\Sigma_{\mathrm{c}}^{\mathrm{r}}] \quad f_{\mathrm{c}}(E) \tag{5}$$

$$\Sigma_{\mathrm{c}}^{>}(E) = +2i\Im m[\Sigma_{\mathrm{c}}^{\mathrm{r}}] \quad (1 - f_{\mathrm{c}}(E)), \tag{6}$$

where τ is the coupling matrix between the device and the contact, $f_c(E)$ is the Fermi-Dirac distribution function at the contact c, and g_c is the surface Green's function. The calculation of the surface Green's function is described in Refs. [3,8,23].

2.3. Scattering self-energies

Using a perturbation expansion one can define the self-energy Σ as an irreducible part of the Green's function. An exact evaluation of the self-energy is possible only for some rather pathological models. For real systems one has to rely on approximation schemes. In this work, the lowest-order self-energy for electron–phonon interaction within the self-consistent Born approximation has been applied [3]. The self-energy due to electron–phonon interaction comprises the contributions of elastic and inelastic scattering mechanisms, $\Sigma_{\text{e-ph}} = \Sigma_{\text{el}} + \Sigma_{\text{inel}}$. The interaction of electrons with optical phonons is inelastic. Assuming that the interaction occurs locally [15], $\Sigma(z, z'; E) = 0$ for $z \neq z'$, the self-energies can be written as

$$\Sigma_{\mathrm{inel}}^{<}(E) = \sum_j D_{\mathrm{inel},j} \left[(n_B(\hbar\omega_j) + 1) G^{<}(E + \hbar\omega_j) + n_B(\hbar\omega_j) G^{<}(E - \hbar\omega_j) \right], \tag{7}$$

$$\Sigma_{\mathrm{inel}}^{>}(E) = \sum_j D_{\mathrm{inel},j} \left[(n_B(\hbar\omega_j) + 1) G^{>}(E - \hbar\omega_j) + n_B(\hbar\omega_j) G^{>}(E + \hbar\omega_j) \right], \tag{8}$$

where $\hbar\omega_j$ denotes the phonon energy of branch j, $n(\hbar\omega_j)$ the average phonon occupation number, and D_j the electron–phonon coupling strength. Assuming that the bath of phonons is maintained in thermodynamic equilibrium, $n(\hbar\omega_j)$ is given by

$$n(\hbar\omega_j) = \frac{1}{\exp(\hbar\omega_j / k_{\mathrm{B}}T) - 1}. \tag{9}$$

The electron–phonon interaction strength for a $(n, 0)$ zigzag CNT is given by

$$D_{\mathrm{inel},j} = \frac{\hbar |M_j|^2}{2n m_{\mathrm{c}} \omega_j}, \tag{10}$$

where m_{c} is the mass of a carbon atom, and M_j are the matrix elements of the electron–phonon interaction Hamiltonian [20] which depend on the chirality and the diameter of the CNT [17]. Interaction with acoustic phonons can be regarded as elastic scattering, $E \pm \hbar\omega_j \approx E$. Based on this approximation, the self-energies for acoustic phonon interaction simplify to

$$\Sigma_{\mathrm{el}}^{\lessgtr}(E) = D_{\mathrm{el}} G^{\lessgtr}(E), \tag{11}$$

$$D_{\mathrm{el},j} = \frac{k_{\mathrm{B}} T |M_j|^2}{n m_{\mathrm{c}} \upsilon_j}, \tag{12}$$

where υ_j is the velocity of the acoustic phonon. The retarded self-energy is given by

$$\Sigma^{\mathrm{r}}_{\text{el-ph}}(E) = -\frac{i}{2}\Gamma_{\text{el-ph}}(E) + P\int \frac{\mathrm{d}E'}{2\pi}\frac{\Gamma_{\text{el-ph}}(E')}{E-E'}, \tag{13}$$

where $\Gamma_{\text{el-ph}} \equiv i(\Sigma^{>}_{\text{el-ph}} - \Sigma^{<}_{\text{el-ph}})$ defines the broadening and $P\int$ represents the principal part of the integration. The imaginary part of the retarded self-energy broadens the density of states, whereas the real part shifts it in energy.

2.4. Poisson equation

The electron–electron interaction self-energy of lowest order corresponds to the Hartree potential, which is the solution of the Poisson equation

$$\frac{\partial^2 V}{\partial \rho^2} + \frac{1}{\rho}\frac{\partial V}{\partial \rho} + \frac{\partial^2 V}{\partial z^2} = -\frac{Q}{\epsilon}. \tag{14}$$

For accurate analysis it is essential to solve the coupled system of transport and Poisson equations self-consistently [12,27]. Since an azimuthal symmetric structure is considered, the Poisson Eq. (14) is restricted to two-dimensions. $V(\rho, z)$ is the electrostatic potential, and Q is the space charge density. The boundary conditions for V are given by [12]

$$V(\rho = \rho_{\mathrm{G}}) = \frac{V_{\mathrm{GS}} - \phi_{\mathrm{G}}}{q}, \tag{15}$$

$$V(z = z_{\mathrm{S}}) = -\frac{\phi_{\mathrm{S}}}{q}, \tag{16}$$

$$V(z = z_{\mathrm{D}}) = \frac{V_{\mathrm{DS}} - \phi_{\mathrm{D}}}{q}, \tag{17}$$

where ϕ_{G}, ϕ_{S}, and ϕ_{D} represent the work functions of the gate, source, and drain contacts, respectively. V_{GS} and V_{GD} are the gate-source and drain-source voltages, respectively. The space charge density in (14) is given by [12]

$$Q(\rho, z) = \frac{q(p(z) - n(z))\delta(\rho - \rho_{\mathrm{CNT}})}{2\pi\rho}, \tag{18}$$

where n and p are total electron and hole concentrations per unit length. In (18) δ/ρ is the Dirac delta function in cylindrical coordinates, implying that carrier density is approximated by a sheet charge distributed uniformly over the circumference of the CNT [12]. The electron concentration is calculated from the lesser Green's function as

$$n(z) = -2i\int G^{<}(z, z; E)\frac{\mathrm{d}E}{2\pi}. \tag{19}$$

The hole concentration is calculated in analogy with (19).

3. Numerical solution

In this section the discretization of the equations of both the spatial and energy domain is described. Then the iterative method for solving the system of coupled non-linear equations is presented.

3.1. Discretization of the spatial domain

An equidistant spatial grid is employed. In (1) an effective mass Hamiltonian is assumed. Discretization of the effective mass Hamiltonian with finite differences gives the following matrix:

$$H = \begin{pmatrix} U_1+2t & -t & 0 & 0 & 0 & 0 \\ -t & U_2+2t & -t & 0 & 0 & 0 \\ 0 & \cdots & \cdots & 0 & 0 & 0 \\ 0 & 0 & 0 & \cdots & \cdots & 0 \\ 0 & 0 & 0 & -t & U_{n-1}+2t & -t \\ 0 & 0 & 0 & 0 & -t & U_n+2t \end{pmatrix} \tag{20}$$

Here U_j is the potential energy at some point j, $t = \hbar^2/2m^*a^2$ determines the coupling between neighboring sites, and a is the grid spacing. The wavefunction of carriers with high kinetic energy have a rapidly oscillating behavior. The finite difference approximation to the second derivative operator is accurate only if the wavefunction varies slowly enough on a scale of a. By discretizing the effective mass Hamiltonian the analytical dispersion relation $E(k) = \hbar^2k^2/(2m^*)$, where k is the electron wavevector, follows a cosine function $E(k) = 2t(1 - \cos(ak))$. The two are equivalent only if $(ak) \ll 1$ so that $\cos(ka) \approx 1 - (ka)^2/2$. Considering an effective mass of $m^* \approx 0.05$ m, a grid spacing of about $a \approx 1$ Å satisfies the required condition. Discretized Eqs. (1) and (2) are solved by using a recursive Green's function method [24].

3.2. Selection of the energy grid

The discretization of energy requires more care. The integral (19) has to be evaluated numerically. Therefore, the energy grid should be selected so that the numerical error in evaluating (19) is below a desired limit. There is a wide range of methods available for numerical integration [4]. Adaptive strategies divide the integration interval into sub-intervals and, typically, employ a progressive formula in each sub-interval with some fixed upper limit on the number of points. If the required accuracy is not achieved by the progressive formula, the sub-interval is bisected and a similar procedure carried out on each half. This sub-division process is carried out recursively until the desired accuracy is achieved. In adaptive quadrature algorithms the error estimate governs the decision on whether to accept the current approximation and terminate or to continue. Therefore, both the efficiency and the reliability depend on the error estimation algorithm. The decision to further subdivide a region may be based either on local or on global information. Local information refers only to the region currently being processed, while global information refers to data of the whole region. Integration programs based on global subdivision strategies proved to be more efficient and reliable. In this work a global error estimator based on the *null rules* method has been employed [5]. Applying the adaptive method, the self-consistent simulation converges relatively fast and the simulation time is considerably reduced. Details have been presented in Ref. [21].

3.3. Iterative solution of the non-linear equation system

The Green's functions depend on the electron–phonon self-energies and electrostatic potential. These quantities again depend on the Green's functions. The system of coupled equations can be solved by iteration. First the Green's functions and the electron–phonon self-energies are iterated. After convergence of the electron–phonon self energies, which results in a self-consistent Born approximation [3], the Poisson equations is solved once. Based on the updated electrostatic potential, the Green's functions and the electron–phonon self-energies are iterated again, see Fig. 2. These two iterations continue till a convergence criterion is satisfied. Then, total current through the device is calculated.

4. The effect of electron–phonon interaction parameters

In this section the effects of the parameter values for the electron–phonon coupling strength and the phonon energy on the static response of CNTFETs are investigated. All simulations were performed for the structure shown in Fig. 1.

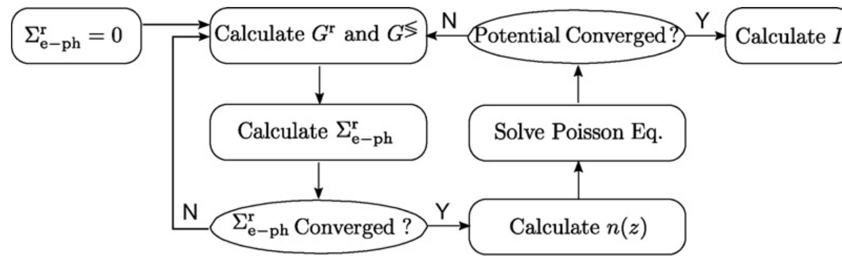

Fig. 2. Block diagram of the iterative procedure employed to solve the coupled system of transport and Poisson equations. For the first step an initial guess for the electron–phonon self-energy is required.

To compare the effect of different scattering mechanisms, we define the ballisticity as the ratio of the current in the presence of electron–phonon interaction to the current in the ballistic case (I_{Sc}/I_{Bl}). Fig. 3 a shows the ballisticity versus $D_{el,inel}$. Elastic scattering conserves the energy of carriers as in the ballistic case, but the current decreases due to elastic back-scattering of carriers. With inelastic scattering the energy of carriers is not conserved. Carriers which acquire enough kinetic energy can emit phonons and scatter into lower energy states. Fig. 3 a shows that the variation of ballisticity versus D_{inel} strongly depends on the phonon energy. For a better comparison Fig. 3 b shows the ballisticity versus phonon energy. With the increase of phonon energy the ballisticity increases, since scattered carriers lose more kinetic energy and the probability for back-scattering decreases [9]. As the phonon energy increases the occupation number (9) decreases exponentially. Therefore, the self-energy decreases and the current is weakly affected even for strong electron–phonon coupling.

All the above discussed results were calculated for a device with a CNT length of 50 nm. In case of ballistic transport the current is independent of the device length, but in the presence of scattering it reduces as the device length increases. Fig. 4 shows the ballisticity as a function of the CNT length in the presence of elastic and inelastic electron–phonon interaction. An artificially large value for the electron–phonon coupling strength and a small value for the phonon energy is chosen to simulate the diffusive limit. In this case, the current is expected to be inversely proportional to the device length according to Ohm's law.

electron–phonon interaction reduces the on-current, both, directly and indirectly [9,6]. The direct effect is due to back-scattering of carriers, but scattering also redistributes the carrier concentration profile along the device. This redistribution affects the band-edge profile so that it reduces the total current. To reduce the indirect effect one should increase the gate–CNT coupling. The electrostatic potential on the surface of the CNT in the middle of the device (neglecting the effect of the source and drain potentials) can be estimated by:

$$V(\rho = \rho_{\rm CNT}) = \left(\frac{V_{\rm GS} - \phi_{\rm G}}{q}\right) \frac{C_{\rm Ins}}{C_{\rm Ins} + C_{\rm Q}}, \tag{21}$$

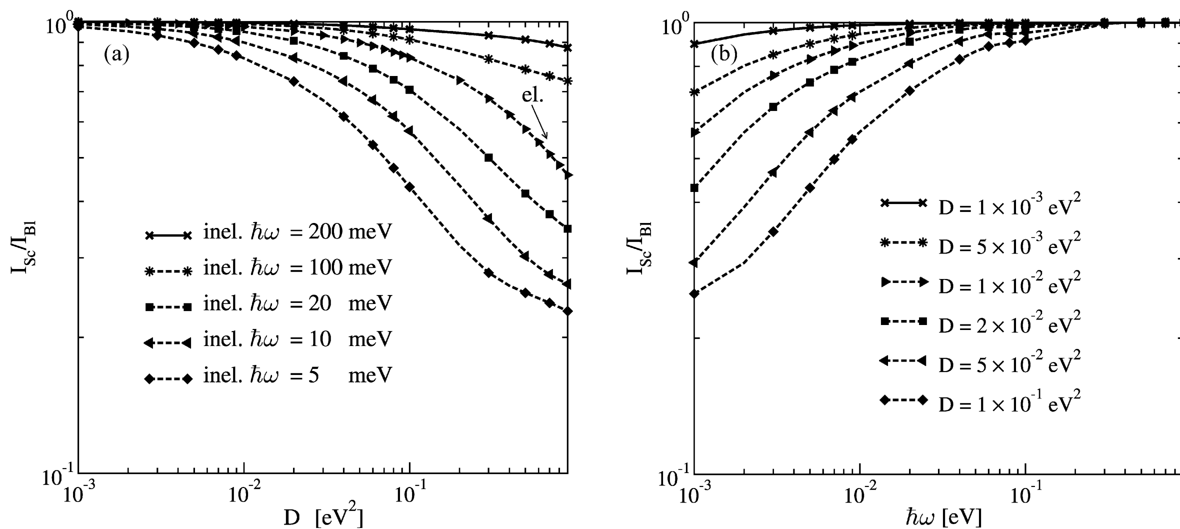

Fig. 3. (a) Ballisticity versus the electron–phonon coupling strength ($D_{el,inel}$). (b) Ballisticity versus phonon energy ($\hbar\omega_{\nu}$) for inelastic scattering.

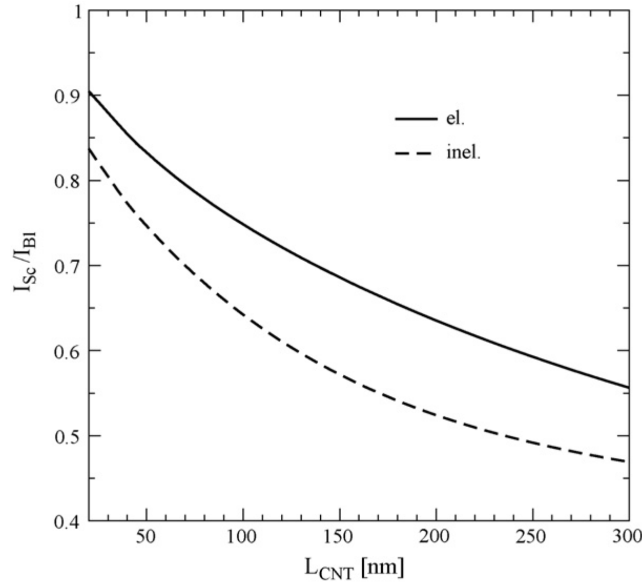

Fig. 4. Ballisticity versus CNT length. $D = 10^{-1}\,\mathrm{eV}^2$ for both elastic and inelastic scattering and $\hbar\omega = 25\,\mathrm{meV}$ for inelastic scattering. These scattering parameters simulate the diffusive regime. In this case the ballisticity is inversely proportional to the device length.

where C_{Ins} is the insulator capacitance and C_{Q} is the quantum capacitance. The latter is given by $C_{\mathrm{Q}} = 8q^2/h\nu_{\mathrm{F}} \approx 400\,\mathrm{aF}/\mu\mathrm{m}$, including the twofold band and spin degeneracy [2,13]. If thin high-κ insulators are used, $C_{\mathrm{Ins}} \gg C_{\mathrm{Q}}$, the potential on the surface of the CNT becomes equal to the gate potential (perfect coupling). This regime is called quantum capacitance limit in which the device is potential-controlled rather than charge-controlled [7]. Fig. 5 compares the ballisticity for different insulators. The proportions of the direct and indirect effect of scattering on the on-current are shown. For the given material and geometrical parameters a value of $\kappa > 20$ suppresses the indirect effect of scattering.

5. Electron–phonon interaction parameters in CNTs

In general the electron–phonon interaction parameters depend on the diameter and the chirality of the CNT. The theoretical calculation of these parameters has been reported in Refs. [17,20]. The band gap of a semiconducting

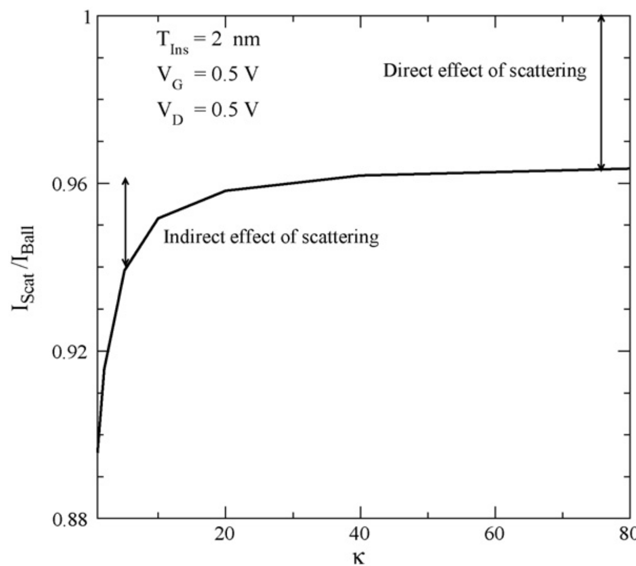

Fig. 5. The ratio of the drain current in the presence of scattering to that in the ballistic limit for different κ. The fractions due to the direct and the indirect effects of scattering on the on-current are shown. For a high- κ insulator the indirect part decreases.

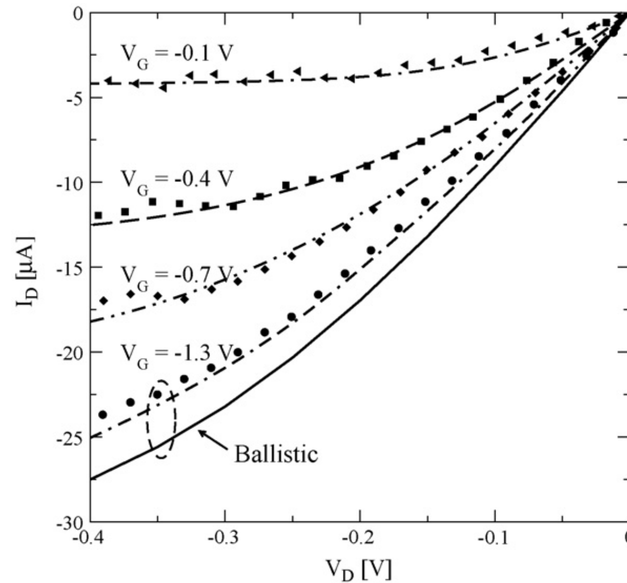

Fig. 6. Comparison of the simulation results and experimental data [10] for the output characteristics of a p-channel CNTFET. The results for the bias point $V_G = -1.3$ V are compared with the ballistic limit.

CNT is inversely proportional to the diameter. A rough estimate is $E_G = 0.8\,\text{eV}/d_{CNT}$ nm. CNTs with a diameter $d_{CNT} > 2$ nm have a band gap $E_G < 0.4$ eV, which render them unsuitable as transistor channels. Since the fabrication of devices with a diameter $d_{CNT} < 1$ nm is very difficult, we limit our study to zigzag CNTs with diameters in the range d_{CNT} =1–2 nm.

For intra-valley processes, most of the phonons have $q \approx 0$ and are referred to as Γ-point phonons. Γ-point phonons belong to the twisting acoustic (TW), the longitudinal the acoustic (LA), the radial breathing mode (RBM), the out-of-phase out-of-plane optical branch (ZO), the transverse optical (TO), or the longitudinal optical (LO) phonon branch. Phonons inducing inter-valley processes have a wavevector of $|q| \approx q_K$, where q_K corresponds to the wavevector of the K-point of the Brillouin zone of graphene. K-point phonons, also referred to as zone boundary phonons, are a mixture of fundamental polarizations [14].

Acoustic phonons scattering is treated as an elastic process. Inelastic scattering is induced by LO, RBM, and K-point phonon modes. Considering the class of CNTs discussed above, the energies of the these phonon modes are $\hbar\omega_{LO} \approx 200$ meV, $\hbar\omega_{RBM} \approx 30$ meV, and $\hbar\omega_{K_1} \approx 160$ meV, and $\hbar\omega_{K_2} \approx 180$ meV [19,14]. The corresponding coupling coefficients are $D_{LO} \approx 40 \times 10^{-3}\,\text{eV}^2$, $D_{RBM} \approx 10^{-3}\,\text{eV}^2$, and $D_{K_1} \approx 10^{-4}\,\text{eV}^2$, and $D_{K_2} \approx 50 \times 10^{-3}\,\text{eV}^2$ [17,14].

As discussed in Section 4, high energy phonons, such as LO and K-point phonons, reduce the on-current only weakly. Low energy phonons, such as the RBM phonon, can reduce the on-current more effectively. However, due to weak coupling the RBM phonon has a negligible effect at room temperature. The electron–phonon coupling is also weak for acoustic phonons ($D_{AP} < 10^{-3}\,\text{eV}^2$), which implies that elastic back-scattering of carriers is weak. Therefore, the on-current of short CNT based transistors can be close to the ballistic limit [10]. Fig. 6 shows excellent agreement between simulation results and experimental data [10]. The result for the bias point $V_G = -1.3$ V is compared with the ballistic limit, which confirms the validity of nearly ballistic transport in short CNTFETs.

6. Conclusions

Based on the NEGF formalism we investigated the effect of electron–phonon interaction on the performance of CNTFETs. For elastic scattering the electron–phonon coupling strength plays an important role. For inelastic scattering not only the coupling strength, but also the phonon energy is an important factor. In CNTs relevant for FETs, either the electron–phonon coupling is weak or the phonon energies are high. Therefore, the performance of short devices is only weakly affected.

Acknowledgments

This work, as part of the European Science Foundation EUROCORES Programme FoNE, was supported by funds from FWF (contract I79-N16), CNR, EPSRC and the EC Sixth Framework Programme, under Contract N. ERAS-CT-2003-980409.

References

[1] J. Appenzeller, M. Radosavljevic, J. Knoch, P. Avouris, Tunneling versus thermionic emission in one-dimensional semiconductors, Phys. Rev. Lett. 92 (2004) 048301–048304.
[2] P. Burke, AC performance of nanoelectronics: towards a ballistic THz nanotube transistors, Solid State Electron. 48 (10/11) (2004) 1981–1986.
[3] S. Datta, Electronic Transport in Mesoscopic Systems, Cambridge University Press, New York, 1995.
[4] P. Davis, P. Rabinowitz, Methods of Numerical Integration, second ed., Academic Press, Orlando, 1984.
[5] T. Espelid, Adaptive doubly quadrature routines based on Newton–Cotes rules, BIT 43 (2) (2003) 319–337.
[6] J. Guo, A quantum-mechanical treatment of phonon scattering in carbon nanotube transistors, J. Appl. Phys. 98 (2005), 063519-6.
[7] J. Guo, S. Datta, M. Lundstrom, Assesment of silicon MOS and carbon nanotube FET performance limits using a general theory of ballistic transistors, IEDM Tech. Dig., San Francisco, 2002, pp. 711–714.
[8] J. Guo, S. Datta, M. Lundstrom, M. Anantram, Multi-scale modeling of carbon nanotube transistors, Int. J. Multiscale Comput. Eng. 2 (2) (2004) 257–278.
[9] J. Guo, M. Lundstrom, Role of phonon scattering in carbon nanotube field-effect transistors, Appl. Phys. Lett. 86 (2005), 193103-3.
[10] A. Javey, J. Guo, D. Farmer, Q. Wang, E. Yenilmez, R. Gordon, M. Lundstrom, H. Dai, Self-aligned ballistic molecular transistors and electrically parallel nanotube arrays, Nano Lett. 4 (7) (2004) 1319–1322.
[11] A. Javey, J. Guo, Q. Wang, M. Lundstrom, H. Dai, Ballistic carbon nanotube field-effect transistors, Nature (London) 424 (6949) (2003) 654–657.
[12] D. John, L. Castro, P. Pereira, D. Pulfrey, A. Schrödinger-Poisson, Solver for modeling carbon nanotube FETs, in: Proceedings of NSTI Nanotechnology, vol. 3, Boston, 2004, pp. 65–68.
[13] D. John, L. Castro, D. Pulfrey, Quantum capacitance in nanoscale device modeling, J. Appl. Phys. 96 (9) (2004) 5180–5184.
[14] S.O. Koswatta, S. Hasan, M. Lundstrom, M. Anantram, D.E. Nikonov, Ballisticity of nanotube FETs: role of phonon energy and gate bias, Appl. Phys. Lett. 89 (2006), 023125-3.
[15] R. Lake, S. Datta, Nonequilibrium Green's-function method applied to double-barrier resonant-tunneling diodes, Phys. Rev. B 45 (12) (1992) 6670–6685.
[16] R. Lake, G. Klimeck, R.C. Bowen, D. Jovanovic, Single multiband modeling of quantum electron transport through layered semiconductor devices, J. Appl. Phys. 81 (12) (1997) 7845–7869.
[17] G.D. Mahan, Electron-optical phonon interaction in carbon nanotubes, Phys. Rev. B 68 (2003) 125409–125415.
[18] R. Martel, T. Schmidt, H. Shea, T. Hertel, P. Avouris, Single-and multi-wall carbon nanotube field-effect transistors, Appl. Phys. Lett. 73 (17) (1998) 2447–2449.
[19] J. Park, S. Rosenblatt, Y. Yaish, V. Sazonova, H. Ustunel, S. Braig, T. Arias, P. Brouwer, P. McEuen, Electron–phonon scattering in metallic single-walled carbon nanotubes, Nano Lett. 4 (3) (2004) 517–520.
[20] V.N. Popov, P. Lambin, Intraband electron–phonon scattering in single-walled carbon nanotubes, Phys. Rev. B 74 (2006), 075415-13.
[21] M. Pourfath, H. Kosina, S. Selberherr, Rigorous modeling of carbon nanotube transistors, IOP J. Phys.: Conf. Ser. 38 (2006) 29–32.
[22] R. Saito, G. Dresselhaus, M. Dresselhaus, Physical Properties of Carbon Nanotubes, Imperial College Press, London, 1998.
[23] A. Svizhenko, M. Anantram, Effect of scattering and contacts on current and electrostatics in carbon nanotubes, Phys. Rev. B 72 (2005), 085430-10.
[24] A. Svizhenko, M. Anantram, T.R. Govindan, B. Biegel, R. Venugopal, Two-dimensional quantum mechanical modeling of nanotransistors, J. Appl. Phys. 91 (4) (2002) 2343–2354.
[25] W. Tian, S. Datta, S. Hong, R. Reifenberger, J.I. Henderson, C.P. Kubiak, Conductance spectra of molecular wires, J. Chem. Phys. 109 (7) (1998) 2874–2882.
[26] R. Venugopal, Z. Ren, S. Datta, M. Lundstrom, D. Jovanovic, Simulating quantum transport in nanoscale transistors: real versus mode-space approaches, J. Appl. Phys. 92 (7) (2002) 3730–3739.
[27] F. Zahid, A. Ghosh, M. Paulsson, E. Polizzi, S. Datta, Charging-induced asymmetry in molecular conductors, Phys. Rev. B 70 (2004), 245317-5.